Molecules and Cells

Minireview

Recent Developments in Correlative Super-Resolution Fluorescence Microscopy and Electron Microscopy

Dokyung Jeong[1] and Doory Kim[1,2,3,4,*]

[1]Department of Chemistry, Hanyang University, Seoul 04763, Korea, [2]Research Institute for Convergence of Basic Sciences, Hanyang University, Seoul 04763, Korea, [3]Institute of Nano Science and Technology, Hanyang University, Seoul 04763, Korea, [4]Research Institute for Natural Sciences, Hanyang University, Seoul 04763, Korea
*Correspondence: doorykim@hanyang.ac.kr
https://doi.org/10.14348/molcells.2021.5011
www.molcells.org

The recently developed correlative super-resolution fluorescence microscopy (SRM) and electron microscopy (EM) is a hybrid technique that simultaneously obtains the spatial locations of specific molecules with SRM and the context of the cellular ultrastructure by EM. Although the combination of SRM and EM remains challenging owing to the incompatibility of samples prepared for these techniques, the increasing research attention on these methods has led to drastic improvements in their performances and resulted in wide applications. Here, we review the development of correlative SRM and EM (sCLEM) with a focus on the correlation of EM with different SRM techniques. We discuss the limitations of the integration of these two microscopy techniques and how these challenges can be addressed to improve the quality of correlative images. Finally, we address possible future improvements and advances in the continued development and wide application of sCLEM approaches.

Keywords: correlative light and electron microscopy, correlative super-resolution fluorescence and electron microscopy, electron microscopy, super-resolution fluorescence microscopy

INTRODUCTION

The light microscope is the most important tool for visualizing the fine details of an object. In light microscopy, an image can be formed through the interactions of light with matter, such as diffraction and interference, and its resolution is thus limited by diffraction. Far-field microscopes have been considered to have reached their resolution limit, which is ~λ/2, due to this diffraction limit. This resolution limit is approximately 200-300 nm in the lateral dimension and 500-700 nm in the axial dimension, resulting from the point spread function, which is larger than those of many subcellular structures. Thus, many biological structures cannot be observed in detail with the diffraction-limited resolution of fluorescence microscopy. To overcome the diffraction barrier, several super-resolution fluorescence microscopy (SRM) techniques have been recently developed, such as stochastic optical reconstruction microscopy (STORM) (Rust et al., 2006), (fluorescence) photoactivation localization microscopy ((F)PALM) (Betzig et al., 2006), stimulated emission depletion (STED) (Hell and Wichmann, 1994), and saturated structured-illumination microscopy (SSIM) (Gustafsson, 2005).These methods enable the observation of previously unresolved details of cellular structures by maintaining neighboring fluorescent molecules in different states (i.e., fluorescent and dark) based on their

Received 28 October, 2021; revised 31 December, 2021; accepted 31 December, 2021; published online 21 January, 2022

eISSN: 0219-1032

physical or chemical properties (Go et al., 2021).

Although SRM techniques increase the spatial resolution by an order of magnitude or even more than the diffraction-limited resolution, they still cannot resolve many cellular structures with a size of a few nanometers. Although the recently introduced MINFLUX (minimal photon fluxes) nanoscopy, which has been developed based on a synergistic combination of the specific strengths of STORM/PALM and STED, has demonstrated spatial resolutions in the range of 1-3 nm for structures, application of such SRM remains limited to mapping the labeled fluorophores, not the real target itself (Gwosch et al., 2020; Schmidt et al., 2021). Such small-sized ultrastructures in cells are often observed by electron microscopy (EM) because transmission and scanning electron microscopy (TEM and SEM, respectively) allow higher resolutions than SRM. These methods also allow subcellular organelles, including lipid membranes, to be imaged at a nanometer resolution without specific labeling, implying that EM can provide spatial information of "reference space." However, molecular-specific imaging is limited by EM, and only a small number of specific molecular structures with characteristic shapes can be identified in EM images. Examples of such structures are the mitochondria, endoplasmic reticulum, and microtubules. In addition, live-cell imaging with EM remains challenging owing to the requirement of an ultra-high vacuum and conductive metal coating during imaging (Kim et al., 2021b).

Because of the complementary advantages and disadvantages of SRM and EM, they have recently been combined to simultaneously obtain the spatial locations of specific molecules with SRM and the context of the cellular ultrastructure revealed by EM, such that we can benefit from the advantages of both techniques. This integration of SRM and EM techniques is often referred to as correlative SRM and EM (sCLEM) (Hauser et al., 2017; Kim et al., 2015). Although the combination of SRM and EM remains challenging owing to the incompatibility of their sample preparations, sCLEM can add new dimensions to SRM techniques by allowing meaningful correlations with ultrastructural details (Hauser et al., 2017; Kim et al., 2015). To obtain multidimensional information from the same target, different types of SRM have been combined with various EM methods. These have been utilized for imaging various cellular targets over the past decade. The sample condition determines the choice of the EM type to be combined with the SRM. For example, for thin samples or for samples for which the surface is of interest, metal replica TEM or SEM imaging of whole-mount samples would work well (Kim et al., 2015). Meanwhile, if the samples are embedded in resins and sectioned using an ultramicrotome, the interior regions of these samples can be imaged by TEM or BSE-SEM (backscattered electron-SEM). To preserve their native ultrastructures, the samples can be cryofixed and cryo-sectioned, instead of being chemically fixed or resin embedded (Ahn et al., 2020).

In this review, we discuss the technological advances in sCLEM depending on their types (STORM, PALM, STED, and SSIM) and their applications to various biological samples. In sCLEM, it is challenging to obtain optimal quality for both SRM and EM because the samples prepared for both imaging methods are not compatible. For example, the strong fixation conditions typically required for ultrastructure preservation in EM sample preparation can result in fluorescence quenching. This results in a degradation in the SRM image quality. However, mild fixation conditions cannot be used to minimize the photon loss of fluorophores, hence ultimately compromising the quality of both SRM and EM. We describe the limitations of these techniques and attempts to overcome these challenges. Lastly, we discuss possible future improvements and advances in sCLEM.

CORRELATIVE SUPER-RESOLUTION FLUORESCENCE MICROSCOPY AND ELECTRON MICROSCOPY

Correlative STORM and EM

STORM employs the stochastic activation of individual fluorescent molecules at different times, allowing spatially resolved single-molecule imaging (Fig. 1A). Given that the fluorescence intensity from a single molecule is the most important factor in determining the resolution of STORM (Kim et al., 2021a), it is important to minimize the photon loss of fluorophores resulting from the strong fixation during EM sample preparation for correlative STORM and EM imaging.

To overcome this limitation, many researchers have performed correlative STORM and EM imaging by separating the fluorescence-incompatible conditions for EM sample preparation from STORM imaging (Chung et al., 2021) (Fig. 1B, Table 1). For instance, Löschberger et al. (2014) first obtained the STORM image of nuclear pore complexes, and then fixed the samples with 2.5% glutaraldehyde (GA) and stained them with 2% osmium tetroxide (OsO_4) for subsequent SEM imaging. Kim et al. (2015) also separated the treatment of fluorescence-quenchable fixation and staining reagents from STORM imaging to obtain high-quality STORM images of virus-infected cells by completely avoiding photon loss in STORM imaging (Fig. 1C). Similarly, Suleiman et al. (2013) reported good quality STORM images for the kidney glomerular capillary loop by fixing samples with 2% GA and depositing platinum to form a replica for EM imaging. By completely separating the fluorescence-incompatible conditions for EM sample preparation, such as strong fixation and metal staining steps from STORM imaging, neither STORM nor EM image quality was compromised although those imaging regions were limited to the surface structures of the samples. Additionally, Wojcik et al. (2015) developed the correlative STORM and SEM method using graphene coating to bypass fluorescence-quenchable EM preparation steps. Graphene-coated wet cell samples could be imaged by both STORM and SEM because graphene is transparent to both light and electrons. Owing to the electrically conductive and liquid-impermeable properties of the graphene layer, the graphene-coated wet cell samples did not need dehydration or coating with a conductive layer for EM imaging. Hence, fluorescence quenching has been avoided. In these methods, most of the sample preparation protocols for STORM and EM were based on standard protocols used for each imaging modality; hence, neither STORM nor EM images were substantially compromised. However, these approaches are limited to imaging structures that are relatively close to the cell surface.

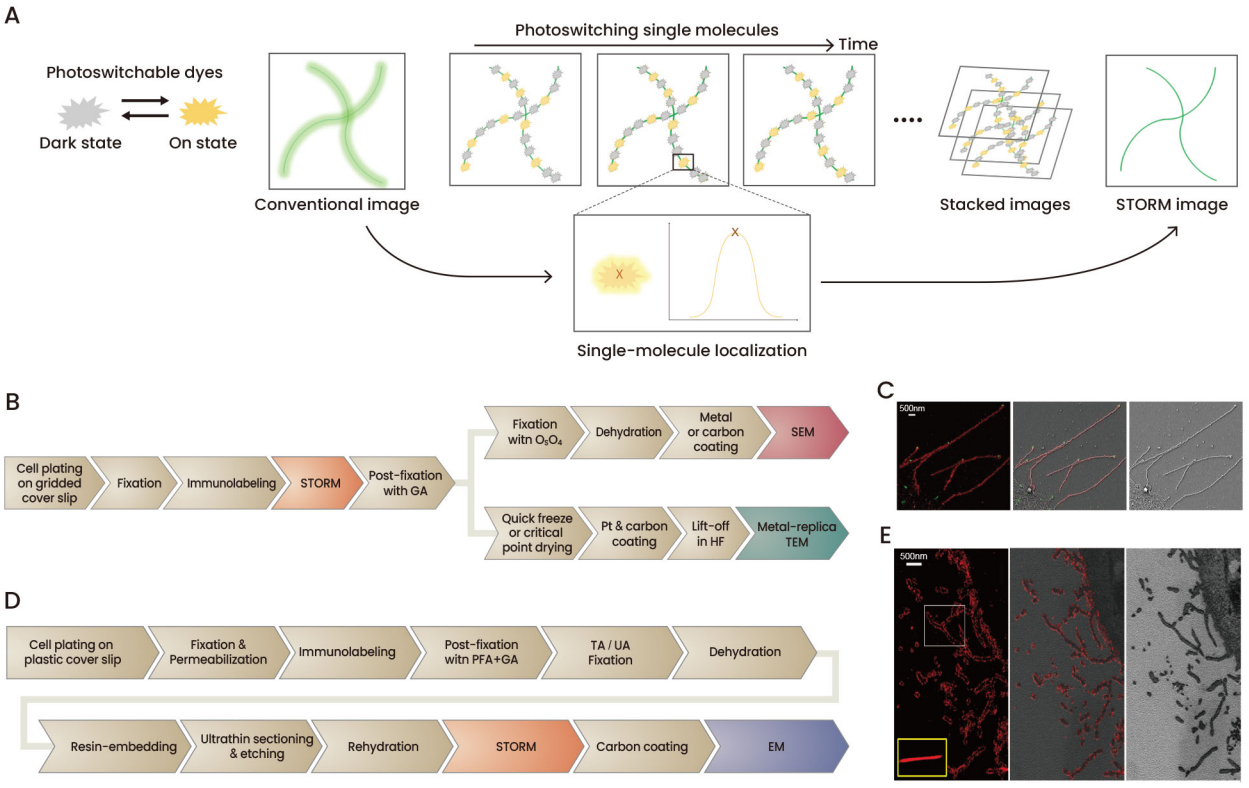

Fig. 1. Recent development in correlative STORM and EM. Correlative STORM and EM (A) The principle of STORM (B) Flowchart of the major steps in correlative STORM and SEM/metal replica TEM imaging of unembedded samples. (C) Correlative STORM and SEM images of individual budding filamentous influenza viruses immunolabeled for M1 (red) and vRNP (green). Left: STORM image. Right: SEM image. Middle: Overlaid image. (D) Flowchart of the major steps in correlative STORM and BSE-SEM/TEM imaging of resin-embedded samples. (E) Correlative STORM and BSE-SEM images of influenza infected A549 cells immuno-stained for HA. Left: STORM image. Right: SEM image. Middle: Overlaid image. (C and E) Adapted from the article of Kim et al. (2015) (PLoS One *10*, e0124581) under Creative Commons Attribution (CC BY) license.

To image the interior regions of thick biological samples, they need to be embedded in resins and thin-sectioned. However, it is challenging to obtain good quality for both STORM and EM imaging with such thin-sectioned samples because an embedding procedure, including strong EM-related fixation, can affect both the fluorescence in STORM images and the ultrastructure preservation in EM images. To minimize these effects, researchers have optimized sample preparation for STORM and EM (Fig. 1D). For example, Perkovic et al. (2014) chose the SiR fluorophore from a screening test of synthetic fluorophores because of its ideal photoswitching properties under a specific buffer, pH, and laser intensities. They also used cryo-fixation without the use of fluorescence-quenchable OsO_4 for resin-embedded section samples. Although they could improve the fluorescence intensity in STORM images under the optimized conditions, the subsequently processed EM image quality substantially degraded owing to insufficient EM fixation. Kim et al. (2015) also developed correlative STORM and EM imaging methods for resin-embedded sectioned samples (Fig. 1E). They tested various types of resins, polymerization strategies, EM fixation additives, and stains to find the ideal conditions to minimize fluorescence quenching and preserve the ultrastructure. They also noticed inhibition of the photoswitching property when the dyes were embedded in resins due to the blocked access of thiol to dye molecules. Because a fast photoswitching rate of the dye molecules is required for super-resolution imaging, they exploited a chemical etching approach to expose the epoxy-embedded dye to the imaging buffer, thereby optimizing photoswitching and improving the quality of super-resolution fluorescence images (Fig. 1E).

Correlative PALM and EM

PALM is a single-molecule localization microscopy technique similar to STORM, and these two techniques are essentially similar in terms of single-molecule localization based method (Jung et al., 2020) (Fig. 2A). Although these techniques currently use both fluorescent organic dyes and fluorescent proteins (FP), we mainly discuss the PALM process that uses FP to focus on its different properties from organic dyes under EM sample preparation. The first correlation of PALM and EM was reported when PALM was first developed, wherein Betzig et al. (2006) showed the application of correlative PALM and TEM for imaging the matrix of mitochondria using

Table 1. Comparison of reported studies on correlative STORM and EM

EM	Sample type in SRM	Sample type in EM	Fluorophore	Target	Remarks	Reference
SEM	Unembedded	Carbon coated	Alexa 647	Nuclear pore complex (NPC) of *Xenopus laevis* oocytes	Symmetric NPC structure used for image correlation	Löschberger et al., 2014
			Alexa 405, Alexa 647	Filamentous influenza viruses infected A549 cells	Photo-etched gridded coverslips	Kim et al., 2015
		Graphene encapsulation	Alexa 647, Cy3B, CM-DiI	Actin, mitochondria in COS-7 cells	Scratch mark on coverslip used for image correlation	Wojcik et al., 2015
		Unembedded	Resorufin	Au-Au nanorod-nanorod and Au-Ag nanorod-nanoparticle catalysts	Symmetric isolated single nanocatalysts used as position markers	Zou et al., 2018
BSE- SEM	Ultrabed resin embedded	Carbon coated	Alexa 647	Filamentous influenza viruses infected A549 cell	Sample prepared on photo-etched gridded coverslips	Kim et al., 2015
TEM	Cryo-sectioned	Metal replica	Alexa 647	Integrin, agrin, collagen, laminin in mouse and human kidney tissue	Gold nanorods deposited coverslips	Suleiman et al., 2013
	Unembedded	Pt/Pd coating	Alexa 647	Microtubule and mitochondria in BS-C-1 cells	Sample prepared on SiN window	Kim et al., 2015
		Unembedded	Atto 647	PLGA-PEG nanoparticles	NPs attached to a copper carbon-coated mesh TEM grid before imaging	Andrian et al., 2021
Cryo-ET	Ultrabed resin embedded	Plunge-frozen in liquid ethane	Alexa 647, Alexa 555	Mouse retina	Fragment applied to carbon coated holey grid before cryo-ET	Robichaux et al., 2019

cryo-section samples (Table 2). The use of cryo-sections allows the FP to preserve their fluorescence intensities, even in the section (Fig. 2B). Kopek et al. (2012; 2013) also used the cryo-section strategy to correlate PALM and SEM (Fig. 2C). Likewise, most correlative PALM and EM imaging has been conducted using cryo-sections, as FP in the cryo-sections remain in the hydrated state at an optimal pH, thus avoiding its destruction and fluorescence quenching. However, the methods that use cryo-sections suffer from a low electron contrast, resulting in low-quality EM images.

To better preserve the ultrastructure of biological samples, correlative cryo-PALM and cryo-EM imaging methods have also been attempted with the recent development of the cryo-imaging technique. Because an elevated temperature at any step can induce the growth of ice crystals, and hence, structural distortion, cryo-PALM imaging after cryofixation allows the samples to remain in their native states in both the PALM and EM images. Although several researchers could obtain high-quality EM images with ultrastructure preservation using this method (Chang et al., 2014; Hoffman et al., 2020; Liu et al., 2015), their PALM images suffered from low labeling density due to the low-resolution effect of cryo-imaging. Although recent studies have made remarkable headway in achieving good quality cryo-PALM images, further improvements in the resolution of cryo-PALM imaging are anticipated to be better correlated with higher resolution EM images (Hoffman et al., 2020).

Another method to preserve the ultrastructure during correlative PALM and EM imaging is the use of resin embedding, which is typically used for the EM imaging of sectioned biological samples (Fig. 2D). Watanabe et al. (2011) developed correlative PALM and BSE-SEM methods based on a conventional resin embedding method. To minimize the fluorescence quenching and destruction of FP, they used a very low concentration of OsO_4 and a hydrophilic acrylic resin. Compared to organic dyes, FP can be easily perturbed by EM fixatives because of the acidic and oxidizing fixation reagents, such as OsO_4; therefore, it is challenging to preserve the fluorescence from FP in the resin-embedded sections. Although Johnson et al. (2015) reported that the fluorescence from mGFP, mVenus, and mRuby2 can be better preserved by the addition of tannic acid, the quality of the PALM image remains poor in the correlative images (Fig. 2E).

To overcome this limitation, various engineered variants of EosFP that fluoresce and photoconvert normally under heavily fixed conditions have been reported. For example, Paez-Segala et al. (2015) developed fixation-resistant mEos4a and mEos4b by reducing the surface side-chain reactivity and improving the thermodynamic stability. They demonstrated that these fixation-resistant Eos variants are

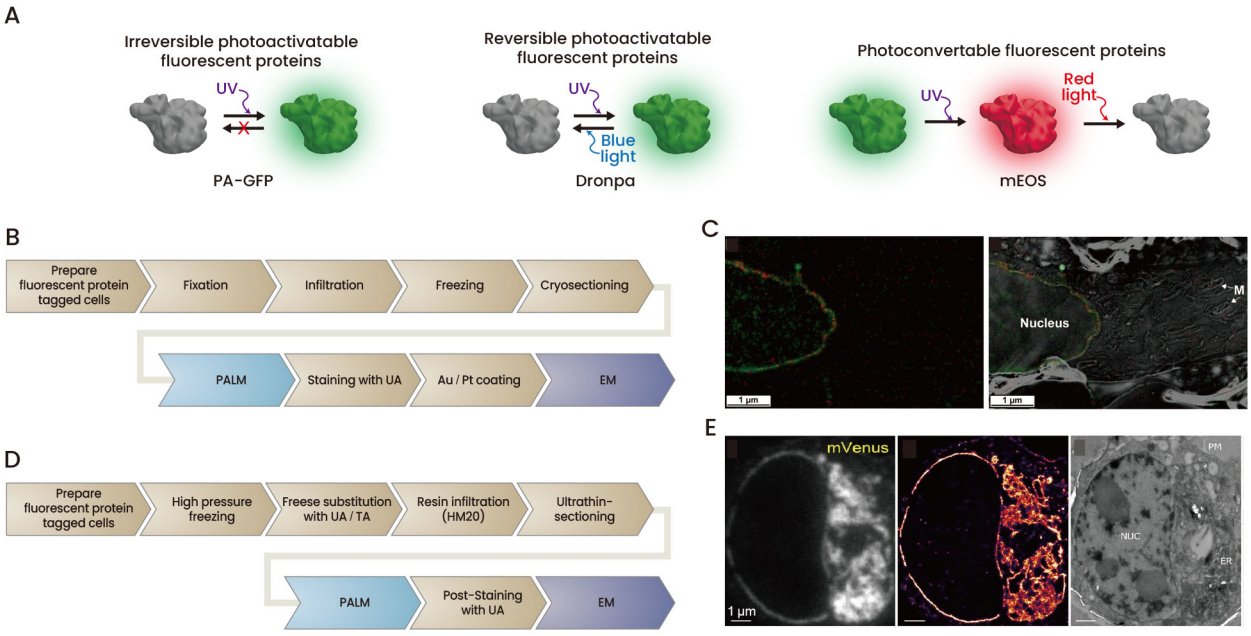

Fig. 2. Recent development in correlative PALM and EM. Correlative PALM and EM (A) The principle of photoactivable FP for PALM (B) Flowchart of the major steps in correlative PALM and EM imaging of cryo-sectioned samples. (C) Correlative PALM and SEM images of nuclear lamina proteins (Lamin A: green, Lamin B1: red). Left: PALM image. Right: Overlaid image. (D) Flowchart of the major steps in correlative PALM and EM imaging of resin-embedded samples. (E) Correlative PALM and TEM images of HEK293T cells transfected with EphA2/A4 receptor proteins fused to mVenus. Left: wide-field image. Middle: PALM image. Right: TEM image. (C) Adapted from the article of Kopek et al. (2013) (PLoS One *8*, e77209) under Creative Commons Attribution (CC BY) license. (E) Adapted from the article of Johnson et al. (2015) (Sci. Rep. *5*, 9583) under Creative Commons Attribution (CC BY) license.

compatible with 0.5%-1% OsO_4-fixed plasticized sections and enable super-resolution imaging. Subsequent work by Fu et al. (2020) also reported another OsO_4-resistant mEos that survived Epon embedding after OsO_4 treatment and reported the improved quality of correlative PALM and EM images for mitochondria and nuclear lamina.

Another method to avoid the fluorescence loss of FP during sample preparations for EM and to preserve the high EM contrast, is to conduct all EM-related sample preparations after PALM imaging, as discussed above. For instance, Van Engelenburg et al. (2014) combined iPALM (interferometric PALM) with SEM to image ESCRT subunits at HIV assembly sites. In addition, Sochacki et al. (2014) employed metal-replica electron tomography for obtaining 3D correlative images with iPALM to completely separate the EM-related sample preparations from those for the iPALM images. Although these methods can avoid the loss of photons or photoactivation properties of FP, the EM images are limited to the cell membrane surface owing to the use of metal replicas and SE-SEM (secondary electron-SEM).

Correlative STED/SSIM and EM

Both STED and SSIM can be categorized as SRM techniques that use patterned illumination; STED uses negative patterning, whereas SSIM uses positive patterning (Fig. 3A). STED microscopy employs the stimulated emission at the area surrounding the focal spot of the excitation laser by the donut-shaped depletion light, allowing a sharpened focal spot of the image. SSIM improves the image resolution up to ~50 nm by the reconstruction of multiple snapshots taken by scanning and rotating the positive patterning of the excitation light on the sample. Because these techniques do not require the photoswitching or photoactivation of fluorophores such as in STORM or PALM, respectively, the quality of STED and SSIM images in the EM correlative images can be less sensitive to the EM-related sample preparation than in those methods (Table 3). For example, Watanabe et al. (2011) reported a better quality of STED images, with higher labeling density than that for the PALM images for mitochondria in their correlation images with BSE-SEM.

There have been substantial efforts to preserve both the fluorescence and ultrastructure of samples when correlating EM with STED or SSIM because they play important roles in determining the quality of SRM and EM images. For instance, de Waal et al. (2018) separated the SSIM imaging step from the EM-related sample preparation steps to image lipopolysaccharide and its association with fibrin fibers, which is similar to the previously discussed correlative STORM/PALM and EM methods. Al Jord et al. (2014) also performed EM-related sample preparation, such as EM-fixation, heavy metal staining, resin embedding, and sectioning, after 3D SIM imaging. To align these two different images for the unsectioned and sectioned sample, they employed gridded coverslips for a reasonable 3D alignment at a high precision. To obtain a high fluorescence

Table 2. Comparison of reported studies on correlative PALM and EM

EM	Sample type in SRM	Sample type in EM	Fluorophore	Target	Remarks	Reference
SEM	Cryo-sectioned	Au/Pd coated	mEos2	Mitochondria in 3T3sw cells	Gold nanospheres deposited and ITO sputtered coverslips	Kopek et al., 2013
	Unembedded	Carbon and Au/PD coated	PSCFP2, Alexa 647	COS-7-HIV Gag-FLAG	Gold nanorods deposited and SiO_2 sputtered coverslips	Van Engelenburg et al., 2014
BSE-SEM	LR White and GMA resin embedded	Carbon coated	Dendra, tdEos	C.elegans worms	High-pressure freezing	Watanabe et al., 2011
	GMA resin embedded	Au/Pd coated	mEos4a, mEos4b	Lamin A in 3T3 cells	High pressure freezing	Paez-Segala et al., 2015
FIB-SEM	Cryo-sectioned	Methylcellulose embedded	mEos2	Mitochondria in 3T3sw cells	Gold fiducial used for image correlation	Kopek et al., 2012
TEM	Cryo-sectioned	Methylcellulose embedded	dEosFP	Mitochondria in COS-7 cells	Stained with 3% uranyl acetate before EM imaging	Betzig et al., 2006
			GFP	Late endosome, lysosome in HT1080 cells	Cryo-sections picked on copper support grids coated with formvar and carbon	Fokkema et al., 2018
	Unembedded	Metal replica, critical-point dried	psCFP2, Alexa 647	Membrane in PC12-GR5 cells	Gold nanorods deposited and SiO_2-sputtered coverslips	Sochacki et al., 2014
		Carbon coated	GFP	Sin1-Dendra2^N	Red-shifted FluoSpheres shows the best performance for correlative PALM and TEM	Fathima et al., 2021
	HM20 resin embedded	HM20 resin embedded	GFP, mVenus, mRuby2	HEK293T cells	High pressure freezing	Johnson et al., 2015
			GFP	E6 Vero cells expressing nsp3-GFP	High pressure freezing	Tuijtel et al., 2017
	Epon resin embedded	Epon resin embedded	mEosEM	Mitochondria in CHO cells	Gold nanoparticles used as markers	Fu et al., 2020
	GMA resin embedded	GMA resin embedded	mEos4a, mEos4b	Lamin A in 3T3 cells	High pressure freezing	Paez-Segala et al., 2015
Cryo-EM	Cryo-sectioned	Cryo-sectioned	Dronpa	Mitochondria in HEK293 cells	High pressure freezing	Liu et al., 2015
Cryo-ET	Plunge frozen	Plunge frozen	PA-GFP	Bacteria (*Myxococcus xanthus*)	PA-GFP photoactivatable at 80K	Chang et al., 2014

intensity from fluorophores, Müller et al. (2017) proposed a protocol for correlative SIM and TEM using self-labeling proteins such as SNAP- and CLIP-tag and organic dyes instead of FP (Figs. 3B and 3C). They demonstrated this protocol for the imaging of age-defined granule morphology and degradation with high fluorescence contrast. Wurm et al. (2019) employed post-embedding immunolabeling rather than pre-embedding immunolabeling to avoid the destructive effects of permeabilization and fluorescence quenching during the embedding process. This method led to a high signal-to-noise ratio of the fluorescence signal; however, the changes in antigenicity resulted in a low labeling density in STED images.

Several dual-contrast reagents have also been developed to better correlate STED/SIM with EM images. For instance, Prabhakar et al. (2018) applied fluorescent nanodiamonds (FNDs) to correlative STED and TEM as dual-contrast fiducial markers because they are known to be EM-detectable electron-dense materials and are compatible with STED imaging (Fig. 3D). Although FNDs allow a resolution of 6 nm during STED imaging, they are limited in their use just as fiducial markers because of the lack of target specificity. As a dual-contrast marker with target specificity, Tian et al. (2020) designed an iridium (III) complex, clr-Tub, which can specifically bind to $\alpha\beta$-tubulin active pockets. They demonstrated the capability of this marker for correlative STED and TEM, but the STED images displayed a limited labeling density for microtubules. As dual-contrast markers are beneficial for providing a precise correlation between SRM and EM images, further developments of such markers to obtain a high labeling density and high binding specificity are necessary for

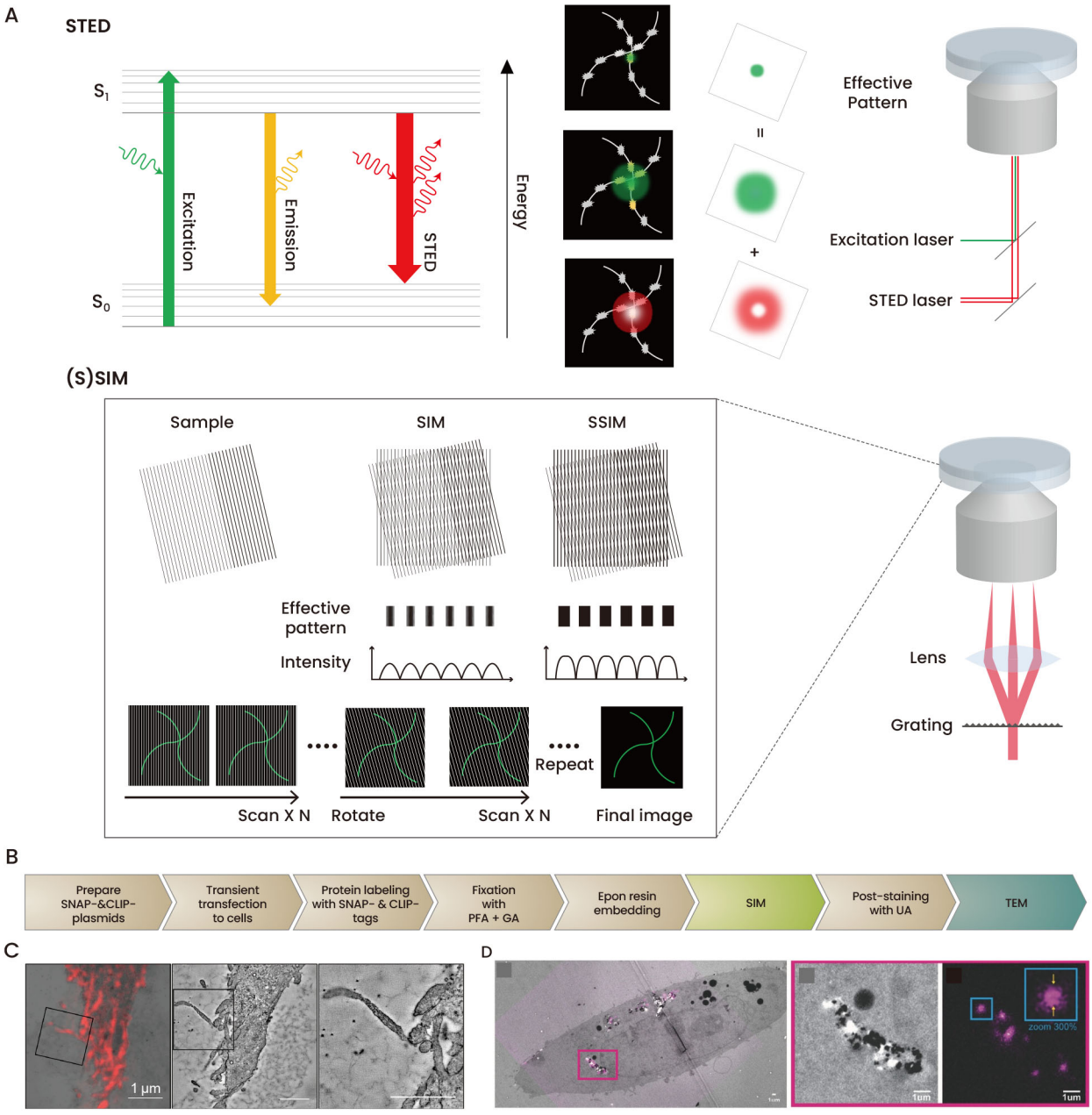

Fig. 3. Recent development in correlative STED/SSIM and EM. Correlative STED/SSIM and EM (A) The principle of STED and SSIM (B) Flowchart of the major steps in correlative SIM and TEM imaging using self-labeling protein tags. (C) Correlative SIM and SEM images of a resin-section of INS-1 cells with TMR and lifeAct-CLIP. Left: Overlaid image. Middle: TEM image. Right: Detail of boxed area in the middle image. Adapted from the article of Müller et al. (2017) (Sci. Rep. *7*, 23) under Creative Commons Attribution (CC BY) license. (D) Correlative STED and TEM imaging of intracellular FNDs in resin sections. Left: Overlaid image. Middle: TEM image of boxed area in the left image. Right: STED image of boxed area in the left image. Adapted from the article of Prabhakar et al. (2018) (Small *14*, 1701807) with original copyright holder's permission.

high-quality correlative images.

PERSPECTIVES ON FUTURE sCLEM IMAGING TECHNIQUES

Considerable attempts have been made to develop sCLEM techniques. This new and fast-growing field of research could be applied in a wide range of areas as it may provide valuable information that has not been obtained through conventional microscopy. In particular, this method has been effectively applied to visualize specific locations of protein coats or viruses on the cell membrane ultrastructure with high mo-

Table 3. Comparison of reported studies on correlative STED/SIM and EM

SRM	EM	Sample type in SRM	Sample type in EM	Fluorophore	Target	Remarks	Reference
STED	SEM	Lowicryl resin embedded	Lowicryl resin embedded	Alexa 594, Atto 590, Abberior STAR RED	Alpha-tubulin and variant surface glycoprotein (VSG), in T.brucei cells	High pressure freezing, Ultrathin sectioning	Wurm et al., 2019
		LR White and GMA resin embedded	Carbon coated	Citrine	*Caenorhabditis elegans* worms	High-pressure freezing	Watanabe et al., 2011
	TEM	Unembedded	Epon resin embedded	MitoTracker Green	Mitochondria	Fluorescent nanodiamonds (FNDs) used as dual contrast marker	Prabhakar et al., 2018
	EF-TEM	Epoxy embedded	Epoxy embedded	cIr-Tub (cyclometalated Iridium (III) complex)	Microtubules in HepG2 cells	Ultrathin sectioning	Tian et al., 2020
SIM	SEM	Unembedded	Carbon coated	Alexa 488	Lipopolysaccharide in whole blood	1% OsO_4 fixation after STORM imaging	de Waal et al., 2018
	FIB-SEM	Cryo-sectioned	Eponate 12 resin embedded, reembedded in durcupan	mEmerald-ER3 JF525, Alexa 647	ER, mitochondria, transferrin in COS-7 cells	High-pressure freezing	Hoffman et al., 2020
	TEM	Cryo-sectioned or epon resin embedded	Methylcellulose embedded or epoxy resin embedded	SNAP	Insulin secretory granules	High pressure freezing	Müller et al., 2017
		Unembedded	Epon resin embedded	Cen2-GFP	Ependymal progenitors	Relocation of grid-imprinted glass	Al Jord et al., 2014
			Araldite resin embedded	Os-1/TeCP ($[Os(phen)_2(dppz)]^{2+}$, Chiral Os(II) Polypyridyl Complexes)	Cell nuclear DNA	Mesh copper grids and fluorescent beads used for correlation	Huang et al., 2020

lecular specificity because the advantages of both SRM and EM images can be obtained without compromised image quality (Bykov et al., 2016; Kim et al., 2015; Sochacki and Taraska, 2021). In addition, the application of this method to nanomedicine is promising. Andrian et al. (2021) recently reported the capability of correlative SRM and TEM to image the functional moieties of nanoparticles at the single-particle level, which is crucial for nanoparticle activity. The technique can be further employed for nonbiological materials, which are generally more robust than biological samples (Hauser et al., 2017). For example, surface-plasmon-enhanced catalytic activity has been visualized by sCLEM at the nanoscale within single plasmonic nanostructures (Zou et al., 2018). By spatially localizing catalytic products using SRM and correlating this with high-resolution nanostructure geometry using EM, nanoscale catalytic properties can be quantified.

Although recent studies have reported promising results using sCLEM as discussed, further improvements are needed to enhance the correlative image quality. First, the precise alignment between SRM and EM images remains challenging owing to the dissimilarity of contrast, spatial resolution, and sample volume owing to shrinkage. Because this constraint arises from the different contrast reagents used for each imaging technique, the use of a dual-contrast reagent could allow improved alignment between the two images with high precision. Although several studies have recently reported the development of dual-contrast correlative imaging agents, including fluorophore-labeled gold nanoparticles, quantum beads, spectrally shifted dark-red FluoSpheres (Fathima et al., 2021), silica-coated gold nanoparticles (Fokkema et al., 2018), uranyl acetate (Tuijtel et al., 2017), FNDs (Prabhakar et al., 2018), and iridium (III) complex (clr-Tub) (Tian et al., 2020), the development of dual-contrast markers with high labeling density, small size, and high binding specificity for diverse targets remains a future challenge. For example, Huang et al. (2020) developed cell-impermeable chiral Os(II) polypyridyl complexes as dual-contrast nuclear DNA imaging reagents. Although they successfully demonstrated the correlative imaging of nuclear DNA with this agent in diffraction-limited LM images, they failed to demonstrate the applicability

of this method for correlative SIM and TEM imaging, probably owing to insufficiently optimized sample preparation for correlation. Because the SRM image quality in the correlative image considerably depends on the fluorescence intensity, as discussed, studies need to optimize sample preparation for better fluorescence preservation when using dual-contrast reagents for sCLEM imaging. Next, it is necessary to overcome the current limitations of sCLEM imaging at a cryo-state as a promising future direction for sCLEM imaging (Jun et al., 2019). Although recent works have demonstrated the feasibility of cryo-SRM imaging and the correlation with cryo-EM, there is still a large resolution gap between cryo-SRM and cryo-EM owing to the limited resolution of SRM images at a cryo-state (Wolff et al., 2016). Such a low resolution of cryo-SRM results from the use of a long-working distance, with nonimmersion objective lenses at a cryo-state. Thus, it is necessary to develop an objective lens that can drastically increase the photon yield in cryo-SRM imaging. In addition, the altered photoswitching or photoactivation properties at a cryo-temperature can limit SRM imaging (Wolff et al., 2016). Therefore, a better understanding of the properties of fluorophores at cryo-temperatures is also needed to optimize the SRM imaging conditions at a cryo-state. The development of SRM at a cryo-state could drive the correlation between cryo-SRM and cryo-electron tomography (cryo-ET). This could enable the 3D visualization of biomolecules and organelles at molecular resolution under close-to-physiological conditions. Although improving the stability of the sample stage and optical aspects in the cryo-imaging setups remain challenging, it is anticipated that structural–functional analyses can be performed in the most innate form of the samples at the nanoscale level (Jun et al., 2019).

Collectively, with the advances in sCLEM, we foresee extensive opportunities for its application to clarify demanding questions in a wide range of areas by providing new and multidimensional information about targets.

ACKNOWLEDGMENTS

This work was supported by the National Research Foundation of Korea (NRF) Grant funded by the Korea government (MSIT) (No. 2021R1C1C1006700) and the POSCO Cheongam Foundation (fellowship to D.K.).

AUTHOR CONTRIBUTIONS

D.K. supervised the overall process and wrote the manuscript, and D.J. designed the figures and the table. All authors discussed the related studies, drafted and contributed to the final manuscript.

CONFLICT OF INTEREST

The authors have no potential conflicts of interest to disclose.

ORCID

Dokyung Jeong https://orcid.org/0000-0003-0616-2943
Doory Kim https://orcid.org/0000-0002-2675-106X

REFERENCES

Ahn, J., Lee, D., Jo, I., Jeong, H., Hyun, J.K., Woo, J.S., Choi, S.H., and Ha, N.C. (2020). Real-time measurement of the liquid amount in cryo-electron microscopy grids using laser diffraction of regular 2-D holes of the grids. Mol. Cells *43*, 298-303.

Al Jord, A., Lemaitre, A.I., Delgehyr, N., Faucourt, M., Spassky, N., and Meunier, A. (2014). Centriole amplification by mother and daughter centrioles differs in multiciliated cells. Nature *516*, 104-107.

Andrian, T., Delcanale, P., Pujals, S., and Albertazzi, L. (2021). Correlating super-resolution microscopy and transmission electron microscopy reveals multiparametric heterogeneity in nanoparticles. Nano Lett. *21*, 5360-5368.

Betzig, E., Patterson, G.H., Sougrat, R., Lindwasser, O.W., Olenych, S., Bonifacino, J.S., Davidson, M.W., Lippincott-Schwartz, J., and Hess, H.F. (2006). Imaging intracellular fluorescent proteins at nanometer resolution. Science *313*, 1642-1645.

Bykov, Y.S., Cortese, M., Briggs, J.A., and Bartenschlager, R. (2016). Correlative light and electron microscopy methods for the study of virus–cell interactions. FEBS Lett. *590*, 1877-1895.

Chang, Y.W., Chen, S., Tocheva, E.I., Treuner-Lange, A., Löbach, S., Søgaard-Andersen, L., and Jensen, G.J. (2014). Correlated cryogenic photoactivated localization microscopy and cryo-electron tomography. Nat. Methods *11*, 737-739.

Chung, J., Jeong, D., Kim, G.H., Go, S., Song, J., Moon, E., Huh, Y.H., and Kim, D. (2021). Super-resolution imaging of platelet-activation process and its quantitative analysis. Sci. Rep. *11*, 10511.

de Waal, G.M., Engelbrecht, L., Davis, T., De Villiers, W.J., Kell, D.B., and Pretorius, E. (2018). Correlative Light-Electron Microscopy detects lipopolysaccharide and its association with fibrin fibres in Parkinson's Disease, Alzheimer's Disease and Type 2 Diabetes Mellitus. Sci. Rep. *8*, 16798.

Fathima, A., Quintana-Cataño, C.A., Heintze, C., and Schlierf, M. (2021). Precision of fiducial marker alignment for correlative super-resolution fluorescence and transmission electron microscopy. Discov. Mater. *1*, 11.

Fokkema, J., Fermie, J., Liv, N., van den Heuvel, D.J., Konings, T.O., Blab, G.A., Meijerink, A., Klumperman, J., and Gerritsen, H.C. (2018). Fluorescently labelled silica coated gold nanoparticles as fiducial markers for correlative light and electron microscopy. Sci. Rep. *8*, 13625.

Fu, Z., Peng, D., Zhang, M., Xue, F., Zhang, R., He, W., Xu, T., and Xu, P. (2020). mEosEM withstands osmium staining and Epon embedding for super-resolution CLEM. Nat. Methods *17*, 55-58.

Go, S., Jeong, D., Chung, J., Kim, G.H., Song, J., Moon, E., Huh, Y.H., and Kim, D. (2021). Super-resolution imaging reveals cytoskeleton-dependent organelle rearrangement within platelets at intermediate stages of maturation. Structure *29*, 810-822.e3.

Gustafsson, M.G. (2005). Nonlinear structured-illumination microscopy: wide-field fluorescence imaging with theoretically unlimited resolution. Proc. Natl. Acad. Sci. U. S. A. *102*, 13081-13086.

Gwosch, K.C., Pape, J.K., Balzarotti, F., Hoess, P., Ellenberg, J., Ries, J., and Hell, S.W. (2020). MINFLUX nanoscopy delivers 3D multicolor nanometer resolution in cells. Nat. Methods *17*, 217-224.

Hauser, M., Wojcik, M., Kim, D., Mahmoudi, M., Li, W., and Xu, K. (2017). Correlative super-resolution microscopy: new dimensions and new opportunities. Chem. Rev. *117*, 7428-7456.

Hell, S.W. and Wichmann, J. (1994). Breaking the diffraction resolution limit by stimulated emission: stimulated-emission-depletion fluorescence microscopy. Opt. Lett. *19*, 780-782.

Hoffman, D.P., Shtengel, G., Xu, C.S., Campbell, K.R., Freeman, M., Wang, L., Milkie, D.E., Pasolli, H.A., Iyer, N., Bogovic, J.A., et al. (2020). Correlative three-dimensional super-resolution and block-face electron microscopy of whole vitreously frozen cells. Science *367*, eaaz5357.

Huang, R., Feng, F.P., Huang, C.H., Mao, L., Tang, M., Yan, Z.Y., Shao, B., Qin, L., Xu, T., Xue, Y.H., et al. (2020). Chiral Os (II) polypyridyl complexes

as enantioselective nuclear DNA imaging agents especially suitable for correlative high-resolution light and electron microscopy studies. ACS Appl. Mater. Interfaces *12*, 3465-3473.

Johnson, E., Seiradake, E., Jones, E.Y., Davis, I., Grünewald, K., and Kaufmann, R. (2015). Correlative in-resin super-resolution and electron microscopy using standard fluorescent proteins. Sci. Rep. *5*, 9583.

Jun, S., Ro, H.J., Bharda, A., Kim, S.I., Jeoung, D., and Jung, H.S. (2019). Advances in cryo-correlative light and electron microscopy: applications for studying molecular and cellular events. Protein J. *38*, 609-615.

Jung, M., Kim, D., and Mun, J.Y. (2020). Direct visualization of actin filaments and actin-binding proteins in neuronal cells. Front. Cell Dev. Biol. *8*, 588556.

Kim, D., Deerinck, T.J., Sigal, Y.M., Babcock, H.P., Ellisman, M.H., and Zhuang, X. (2015). Correlative stochastic optical reconstruction microscopy and electron microscopy. PLoS One *10*, e0124581.

Kim, G.H., Chung, J., Park, H., and Kim, D. (2021a). Single-molecule sensing by grating-based spectrally resolved super-resolution microscopy. Bull. Korean Chem. Soc. *42*, 270-278.

Kim, Y., Kim, T.K., Shin, Y., Tak, E., Song, G.W., Oh, Y.M., Kim, J.K., and Pack, C.G. (2021b). Characterizing organelles in live stem cells using label-free optical diffraction tomography. Mol. Cells *44*, 851-860.

Kopek, B.G., Shtengel, G., Grimm, J.B., Clayton, D.A., and Hess, H.F. (2013). Correlative photoactivated localization and scanning electron microscopy. PLoS One *8*, e77209.

Kopek, B.G., Shtengel, G., Xu, C.S., Clayton, D.A., and Hess, H.F. (2012). Correlative 3D superresolution fluorescence and electron microscopy reveal the relationship of mitochondrial nucleoids to membranes. Proc. Natl. Acad. Sci. U. S. A. *109*, 6136-6141.

Liu, B., Xue, Y., Zhao, W., Chen, Y., Fan, C., Gu, L., Zhang, Y., Zhang, X., Sun, L., Huang, X., et al. (2015). Three-dimensional super-resolution protein localization correlated with vitrified cellular context. Sci. Rep. *5*, 13017.

Löschberger, A., Franke, C., Krohne, G., van de Linde, S., and Sauer, M. (2014). Correlative super-resolution fluorescence and electron microscopy of the nuclear pore complex with molecular resolution. J. Cell Sci. *127*, 4351-4355.

Müller, A., Neukam, M., Ivanova, A., Sönmez, A., Münster, C., Kretschmar, S., Kalaidzidis, Y., Kurth, T., Verbavatz, J.M., and Solimena, M. (2017). A global approach for quantitative super resolution and electron microscopy on cryo and epoxy sections using self-labeling protein tags. Sci. Rep. *7*, 23.

Paez-Segala, M.G., Sun, M.G., Shtengel, G., Viswanathan, S., Baird, M.A., Macklin, J.J., Patel, R., Allen, J.R., Howe, E.S., Piszczek, G., et al. (2015). Fixation-resistant photoactivatable fluorescent proteins for CLEM. Nat. Methods *12*, 215-218.

Perkovic, M., Kunz, M., Endesfelder, U., Bunse, S., Wigge, C., Yu, Z., Hodirnau, V.V., Scheffer, M.P., Seybert, A., Malkusch, S., et al. (2014). Correlative light-and electron microscopy with chemical tags. J. Struct. Biol. *186*, 205-213.

Prabhakar, N., Peurla, M., Koho, S., Deguchi, T., Näreoja, T., Chang, H.C., Rosenholm, J.M., and Hänninen, P.E. (2018). STED-TEM correlative microscopy leveraging nanodiamonds as intracellular dual-contrast markers. Small *14*, 1701807.

Robichaux, M.A., Potter, V.L., Zhang, Z., He, F., Liu, J., Schmid, M.F., and Wensel, T.G. (2019). Defining the layers of a sensory cilium with STORM and cryoelectron nanoscopy. Proc. Natl. Acad. Sci. U. S. A. *116*, 23562-23572.

Rust, M.J., Bates, M., and Zhuang, X. (2006). Sub-diffraction-limit imaging by stochastic optical reconstruction microscopy (STORM). Nat. Methods *3*, 793-796.

Schmidt, R., Weihs, T., Wurm, C.A., Jansen, I., Rehman, J., Sahl, S.J., and Hell, S.W. (2021). MINFLUX nanometer-scale 3D imaging and microsecond-range tracking on a common fluorescence microscope. Nat. Commun. *12*, 1478.

Sochacki, K.A., Shtengel, G., Van Engelenburg, S.B., Hess, H.F., and Taraska, J.W. (2014). Correlative super-resolution fluorescence and metal-replica transmission electron microscopy. Nat. Methods *11*, 305-308.

Sochacki, K.A. and Taraska, J.W. (2021). Find your coat: using correlative light and electron microscopy to study intracellular protein coats. Curr. Opin. Cell Biol. *71*, 21-28.

Suleiman, H., Zhang, L., Roth, R., Heuser, J.E., Miner, J.H., Shaw, A.S., and Dani, A. (2013). Nanoscale protein architecture of the kidney glomerular basement membrane. Elife *2*, e01149.

Tian, X., De Pace, C., Ruiz-Perez, L., Chen, B., Su, R., Zhang, M., Zhang, R., Zhang, Q., Wang, Q., Zhou, H., et al. (2020). A cyclometalated iridium (III) complex as a microtubule probe for correlative super-resolution fluorescence and electron microscopy. Adv. Mater. *32*, e2003901.

Tuijtel, M.W., Mulder, A.A., Posthuma, C.C., van der Hoeven, B., Koster, A.J., Bárcena, M., Faas, F.G., and Sharp, T.H. (2017). Inducing fluorescence of uranyl acetate as a dual-purpose contrast agent for correlative light-electron microscopy with nanometre precision. Sci. Rep. *7*, 10442.

Van Engelenburg, S.B., Shtengel, G., Sengupta, P., Waki, K., Jarnik, M., Ablan, S.D., Freed, E.O., Hess, H.F., and Lippincott-Schwartz, J. (2014). Distribution of ESCRT machinery at HIV assembly sites reveals virus scaffolding of ESCRT subunits. Science *343*, 653-656.

Watanabe, S., Punge, A., Hollopeter, G., Willig, K.I., Hobson, R.J., Davis, M.W., Hell, S.W., and Jorgensen, E.M. (2011). Protein localization in electron micrographs using fluorescence nanoscopy. Nat. Methods *8*, 80-84.

Wojcik, M., Hauser, M., Li, W., Moon, S., and Xu, K. (2015). Graphene-enabled electron microscopy and correlated super-resolution microscopy of wet cells. Nat. Commun. *6*, 7384.

Wolff, G., Hagen, C., Grünewald, K., and Kaufmann, R. (2016). Towards correlative super-resolution fluorescence and electron cryo-microscopy. Biol. Cell *108*, 245-258.

Wurm, C.A., Schwarz, H., Jans, D.C., Riedel, D., Humbel, B.M., and Jakobs, S. (2019). Correlative STED super-resolution light and electron microscopy on resin sections. J. Phys. D Appl. Phys. *52*, 374003.

Zou, N., Chen, G., Mao, X., Shen, H., Choudhary, E., Zhou, X., and Chen, P. (2018). Imaging catalytic hotspots on single plasmonic nanostructures via correlated super-resolution and electron microscopy. ACS Nano *12*, 5570-5579.